

# Quantification of Uncertainty in Thermodynamic Predictions for Vacuum Refining of Liquid Ag–Pb and Au–Pb Binary Alloys

Lesley J. Beyers<sup>a,\*</sup>, Amy Van den Bulck<sup>b</sup>, Bart Blanpain<sup>b</sup>

<sup>a</sup>*Strada Mihai Eminescu 163, Bucharest 020076, Romania*

<sup>b</sup>*KU Leuven, Department of Materials Engineering, Kasteelpark Arenberg 44, bus 2450, 3001 Leuven, Belgium*

---

## Abstract

The common procedure to calculate vapour–liquid equilibrium (VLE) from an ideal gas and activity coefficient model is evaluated. The reliability of these calculations is assessed through a quantification of the uncertainty in the thermodynamic data of Ag–Pb and Au–Pb binary alloys and propagation of this uncertainty in the calculation of a prediction interval for the vapour–liquid equilibrium results. The advantage of this methodology is that all calculated results include an uncertainty interval, which permits an assessment of the impact of the uncertainty in the thermodynamic data and allows for the validation of VLE diagrams with experimental data to be done on a quantitative basis.

*Keywords:* Vapour–liquid equilibrium, Ag–Au–Pb, Liquid alloys, Calculation methodology, Uncertainty propagation

---

## 1. Introduction

. Vacuum metallurgy can be considered a viable alternative to traditional pyrometallurgical processes and exploits the varying tendencies of elements and compounds to form a vapour phase. Vacuum refining of Ag–Au–Pb alloys consists of a vapour–liquid separation in which Pb forms the main component of

---

\*Corresponding author

*Email address:* [lesley.beyers@kuleuven.be](mailto:lesley.beyers@kuleuven.be) (Lesley J. Beyers)

the vapour phase [1, 2, 3] and it competes with alternative approaches, such as cupellation (liquid–liquid separation), the Parkes process [4] and the Davey process [5] (solid–liquid separation). These methods have been used effectively to separate lead from silver and gold, but a further increase in efficiency and separation capability of these processes requires a fundamental understanding of the prevailing mechanisms, availability of reliable thermodynamic data, and suitable modelling tools to predict more favourable operating conditions.

. This paper focuses on the thermodynamics of the vacuum separation process and evaluates the common procedure to calculate vapour–liquid equilibrium (VLE) from an ideal gas and activity coefficient model [6, 7, 8, 3]. The reliability of these calculations is assessed through a quantification of the uncertainty in the thermodynamic data and propagation of this uncertainty in the calculation of a prediction interval for the vapour–liquid equilibrium results. [9] presented an approach that uses the covariance matrix of the least-squares optimisation to calculate the confidence intervals of the obtained phase boundaries in the Bi–Zn and Ag–Sn binary systems. The covariance matrix is an integral part of the least-squares optimisation algorithm [10], but typically not retained for further calculations. In this work, the approach presented by [9] is adapted for use with thermodynamic data [11, 12] that has already been assessed and which has been reported together with its estimated uncertainties for the prediction interval. The methodology is illustrated on the removal of lead from the Ag–Pb and Au–Pb binary alloys. Ag and Au are similar and compatible metals in many respects, but their chemical interaction with Pb differs significantly. The liquid Ag–Pb binary alloy has a positive excess Gibbs energy of mixing i.e. a tendency for phase separation [13], while the liquid Au–Pb binary alloy has a negative excess Gibbs energy of mixing i.e. a tendency for compound formation [14].

## 2. Theory

### 2.1. Vapour–Liquid Equilibria

. Under vacuum conditions, it is reasonable to assume that the vapour phase behaves ideally when in equilibrium with a liquid mixture of non-associating metals. Under the assumption of an ideal vapour phase, the pressure over the liquid Pb–i alloy is given by:

$$p_{\text{tot}} = p_{\text{Pb}} + p_i \quad (1)$$

$$= \gamma_{\text{Pb}} x p_{\text{Pb}}^{\circ} + \gamma_i (1 - x) p_i^{\circ} \quad (2)$$

35 with i either Ag or Au. The total pressure  $p_{\text{tot}}$  and the associated thermodynamic equilibrium are affected by the saturation vapour pressures of the pure components ( $p_i^{\circ}$ ), the liquid mole fraction of Pb ( $x$ ), and the chemical interaction of the components in the liquid phase i.e. their activity coefficients ( $\gamma_i$ ).

. The capacity for vapour–liquid separation of the two components in a binary  
40 alloys can be assessed with the relative volatility

$$\alpha = \frac{\gamma_{\text{Pb}} p_{\text{Pb}}^{\circ}}{\gamma_i p_i^{\circ}} \quad (3)$$

where, by convention, the numerator contains the more volatile component i.e. with higher saturation vapour pressure. For mathematical convenience, the logarithm of the relative volatility is used in this work

$$\log \alpha = \log \left( \frac{\gamma_{\text{Pb}}}{\gamma_i} \right) + \log \left( \frac{p_{\text{Pb}}^{\circ}}{p_i^{\circ}} \right) \quad (4)$$

Mathematically, the reciprocity rule leads to a neutral value of zero with equal  
45 scaling for positive and negative values, and numerically, it avoids several non-linear (logarithmic–exponential) conversions in the calculations. However, the real advantage lies in its clear interpretation of the results:  $\log \alpha = 0$  indicates no thermodynamic driving force for a favourable separation of either component to the vapour phase,  $\log \alpha > 0$  indicates a favourable separation of the more  
50 volatile component to the vapour phase (here Pb), and  $\log \alpha < 0$  indicates the opposite.

## 2.2. Uncertainty Quantification

. The quantification of uncertainty in modelling is based on the law of propagation of uncertainty [15, 16]. If the thermodynamic quantity  $y$  is based on a  
 55 model function

$$y = f(x_1, x_2, \dots, x_n) \quad (5)$$

then the estimated variance of  $y$  is given by

$$u_y^2 = \sum_{i=1}^n \left( \frac{\partial f}{\partial x_i} \right)^2 u_{x_i}^2 + 2 \sum_{i=1}^{n-1} \sum_{j=i+1}^n \frac{\partial f}{\partial x_i} \frac{\partial f}{\partial x_j} u_{x_{ij}} \quad (6)$$

where  $u_{x_i}^2$  is the variance of parameter  $x_i$  and  $u_{x_{ij}}$  the covariance of parameters  $x_i$  and  $x_j$ . The variances and covariances are grouped together as a covariance matrix  $\mathcal{C}$ . The partial derivatives of the model function, often referred to as  
 60 sensitivity coefficients, are conveniently grouped into a sensitivity matrix

$$\mathcal{S}_f = \left[ \begin{array}{cccc} \frac{\partial f}{\partial x_1} & \frac{\partial f}{\partial x_2} & \cdots & \frac{\partial f}{\partial x_n} \end{array} \right]^T \quad (7)$$

. The estimated uncertainty  $u_y$  is directly obtained from the estimated variance of  $y$  and used to define an interval for the uncertainty in the results, represented by an expanded uncertainty  $U_y = k_c u_y$ . A coverage factor  $k_c$  of 2 is used to define the 95 % confidence level of the uncertainty interval [15]. This approach  
 65 is convenient when the input data is obtained as an estimated value and its corresponding uncertainty interval. In the case measured data points are used, standard statistical methods [17] can be used to calculate the 95 % confidence and prediction intervals.

. Using this approach, the uncertainty estimate of  $\log \alpha$  (Eq. 4) is given by

$$u_{\log \alpha} = \sqrt{(u_{\log \gamma_{\text{Pb}}})^2 + (u_{\log \gamma_i})^2 + \left( u_{\log p_{\text{Pb}}}^\circ \right)^2 + \left( u_{\log p_i}^\circ \right)^2} \quad (8)$$

70 where the estimate for  $\log \alpha$  and its associated uncertainty interval is given by:

$$\log \alpha \pm U_{\log \alpha} = \log \alpha \pm k_c u_{\log \alpha} \quad (9)$$

Similar uncertainty expressions can be derived for all quantities used in the calculations. Note that the uncertainty interval of the data used in this study represented the prediction interval. By assuming an undefined, but constant  
75 relative scale between the confidence and prediction intervals, the propagation of uncertainty will yield uncertainty bounds of the prediction interval.

### 3. Thermodynamic Data

#### 3.1. Vapour Pressure of Pure Metals

. The vapour pressure data for silver, gold, and lead are obtained from an  
80 assessment by [11], which is still the recommended dataset in recent compilations [18, 19]. The vapour pressure data is reported as constants for an integrated Clausius–Clapeyron equation:

$$\log p^\circ(\text{atm}) = A + \frac{B}{T} \quad (10)$$

the constants of which are duplicated in Table 1. The equations are claimed to reproduce the vapour pressure within  $\pm 5\%$  and are intended for ideal gases in a  
85 pressure range  $10^{-10}$ – $10^2$  Pa [11]. The estimated uncertainty of the saturation vapour pressure is thus obtained as  $u_{\log p^\circ} = 0.01$ .

Table 1: Vapour pressure parameters from [11]:  $\log p^\circ(\text{atm}) = A + B T^{-1}$ ; 1 atm = 101325 Pa; m.p. = melting point.

	$A$	$B$	T-range (K)
Ag	5.752	-13 827	m.p.–1600
Au	5.832	-18 024	m.p.–2050
Pb	4.911	-9 701	m.p.–1200

#### 3.2. Liquid Binary Alloys

. The activity coefficients of the components are directly related to the excess Gibbs free energy of mixing

$$\Delta G^E = RT(x \ln \gamma_{\text{Pb}} + (1 - x) \ln \gamma_{\text{i}}) \quad (11)$$

90 and their values can be calculated, as a function of temperature and composition, if a suitable expression for  $\Delta G^E$  is obtained from thermodynamic measurement data.

. Thermodynamic data for the liquid alloys is taken from the compilation made by [12], in which thermodynamic quantities and their estimated 95 % uncertainty interval are provided in tabular format at one specific temperature. The 95  
tainty interval are provided in tabular format at one specific temperature. The excess Gibbs free energy of mixing is fitted to the equation of [20]:

$$\Delta G^E = x(1-x)(A + B(1-2x) + Cx(1-x)) \quad (12)$$

. The thermodynamic optimisation is implemented in Python using standard Python 3.6 libraries (NumPy, SciPy, pandas, and matplotlib) [21]. The Levenberg-Marquardt algorithm is used to perform a least-squares optimisation using the  
objective function for the error in  $\Delta G^E$ .  
100

. [12] estimated a 95 % uncertainty interval of  $\pm 100$  cal (418.4 J) at  $x = 0.5$  for both binary systems. This expanded uncertainty corresponds to an estimated uncertainty for the excess Gibbs free energy of 209.2 J at  $x = 0.5$  for both binary systems. The uncertainty value at other compositions is assumed to be of the  
same relative magnitude i.e. scaled proportionally to  $\Delta G_i^E / \Delta G_{0.5}^E$ .  
105

. An identical approach is used to fit the excess entropy of mixing ( $\Delta S^E$ ), where the reported 95 % uncertainty intervals encompass  $\pm 0.464$  J/K (Ag-Pb) and  $\pm 0.502$  J/K (Au-Pb) [12].  $\Delta S^E$  can be treated as the temperature dependence of the excess Gibbs free energy of mixing for a limited temperature  
range. With knowledge of both quantities, it is possible to estimate  $\Delta G^E$  at  
different temperatures, by use of the fundamental thermodynamic definition,  
 $\Delta G^E = \Delta H - T\Delta S^E$ .  
110

## 4. Results and Discussion

### 4.1. Calculated Parameters and their Uncertainty

. The parameters (Eq. 12) for  $\Delta G^E$  and  $\Delta S^E$  for each binary system are listed  
115 in Table 2 and are identical to those of [20].

Table 2: Parameters for Eq. 12.

	$A$	$B$	$C$
	Ag-Pb		1273 K
$\Delta G^E$ (J)	4441	-2740	4312
$\Delta S^E$ (J/K)	4.810	1.798	9.728
	Au-Pb		1200 K
$\Delta G^E$ (J)	-13279	-1416	7706
$\Delta S^E$ (J/K)	10.805	-1.806	-15.186

. Table 3 contains the elements of the covariance matrices for  $\Delta G^E$  and  $\Delta S^E$  for each binary system. Only the lower triangle of the covariance matrix is reported, because of its symmetric nature ( $\mathcal{C}_{ij} = \mathcal{C}_{ji}$ ). Both the polynomial  
120 fit with the reported data points and the estimated uncertainty interval of the thermodynamic data contribute to the values of the elements in the covariance matrix. The latter contribution dominates since the thermodynamic data were reported as optimised data points with an associated uncertainty interval.

Table 3: Lower triangle of the covariance matrix associated with the application of E. 6 to Eq. 12.

	Ag-Pb			Au-Pb		
$\mathcal{C}_{G^E}$	4.53e+05	-	-	9.58e+05	-	-
	-2.80e+05	1.73e+05	-	1.02e+05	1.09e+04	-
	4.40e+05	-2.72e+05	4.27e+05	-5.56e+05	-5.93e+04	3.23e+05
$\mathcal{C}_{S^E}$	0.38	-	-	2.40	-	-
	0.14	0.05	-	-0.40	0.07	-
	0.77	0.29	1.55	-3.37	0.56	4.73

. The sensitivity matrix  $\mathcal{S}$  is derived from the thermodynamic model (Eq. 12)  
125 and its elements depend on whether the thermodynamic quantity of interest is an integral ( $\Delta G^E$ ) or partial ( $\ln \gamma_i$ ) quantity. This matrix can be used together

with the covariance matrix (Table 3) to estimate the uncertainty interval for any of these thermodynamic quantities.

$$U_{GE} = k_c \cdot u_{GE} = k_c \cdot [\mathcal{S}^T \cdot \mathcal{C} \cdot \mathcal{S}]^{1/2} \quad (13)$$

Note that the form of the equation is equivalent to those used for the confidence interval [17, 9].

#### 4.2. Relative Volatility

. The relative volatility takes into account the non-ideal thermodynamic behaviour of the liquid phase and will therefore vary with composition, as illustrated in Figure 1. The value of the relative volatility at constant temperature over the composition range of both binary systems is shown to be sufficiently high to permit an effective removal of Pb to the vapour phase. The figure also illustrates the effect of the mixing properties of the liquid phase. The thermodynamic driving force for the removal of lead from Au–Pb becomes smaller at lower lead concentrations, while the opposite case is observed for Ag–Pb.

. Figure 2 illustrates the effect of temperature on  $\log \alpha$  at  $x = 0.5$  for the Ag–Pb and Au–Pb binary systems. An increase in temperature in both systems leads to a decrease in  $\log \alpha$  i.e. a separation becomes less effective, regardless of the chemical interaction in the liquid. Note that in this calculation, a large extrapolation is done using the assumption of a fixed enthalpy and excess entropy of mixing without a constraint on its impact. These curves can therefore only be considered qualitative and their uncertainty underestimated. A more accurate estimation will require the inclusion of correct high temperature behaviour and measurement data. However, a similar trend is observed in the values reported by [7], calculated with the Molecular Interaction Volume Model (MIVM) for  $\Delta G^E$  and the activity coefficients. The difference between the two sets of predicted values is mainly attributable to use of alternative sources for the saturation vapour pressures. The tabulated  $p_{\text{Au}}^\circ$  of [7] differs by an approximate factor of 2.5, which is consistent with the observed discrepancy. Figure 2

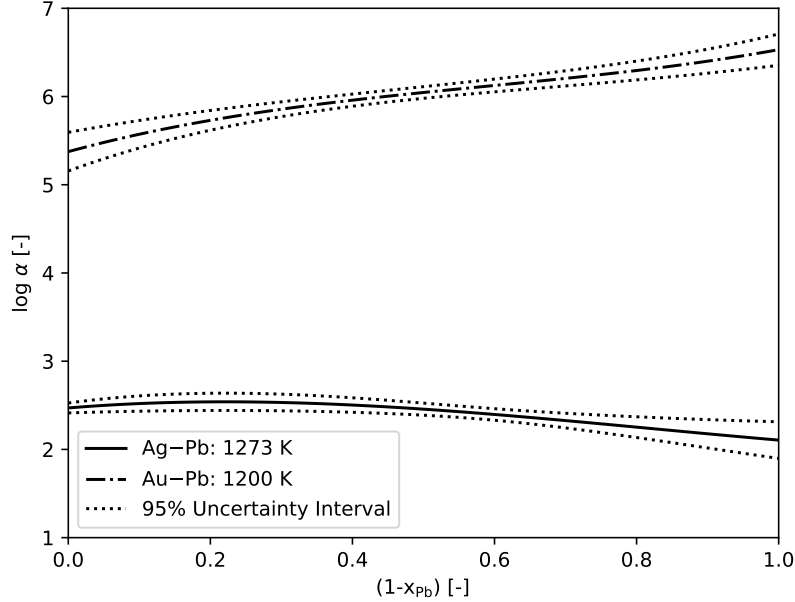


Figure 1: Plot of the relative volatility  $\alpha$  as function of composition for the Ag–Pb and Au–Pb binary system, including the 95 % uncertainty interval, at the temperatures for which the data was compiled.

highlights that the vapour pressure values of the two sources are not compatible,  
 155 according to the reported uncertainties.

#### 4.3. VLE Diagrams

. A second effect of the non-ideal mixing in liquid alloys can be observed by comparing the VLE diagrams for Ag–Pb (Fig. 3) and Au–Pb (Fig. 4). The positive  $\Delta G^E$  leads to a widening of the vapour–liquid coexistence region, while  
 160 the negative  $\Delta G^E$  causes it to narrow compared to an ideal liquid mixture. This widening/narrowing is primarily caused by a shift in the bubble line with the stability of the liquid phase compared to the gas phase; change in the vapour curve is negligible. The 95 % uncertainty interval for the optimised Ag–Pb and Au–Pb systems are indicated in their respective VLE diagrams.

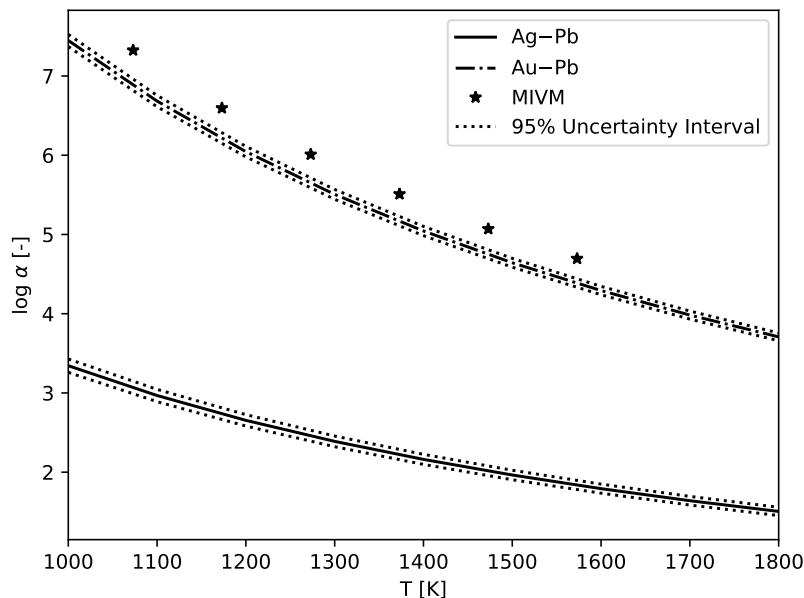


Figure 2: Effect of temperature on the relative volatility  $\alpha$  at  $x=0.5$  for both binary system, including the 95 % uncertainty interval. Values at six temperatures, calculated with the Molecular Interaction Volume Model (MIVM)[7], are shown for Au-Pb.

165 . The Ag-Pb VLE diagram includes the experimental data of Jiang et al. [8] for comparison. Details of the experiment were not provided, but based on the uncertainty intervals indicated here it is doubtful that these measurements are an accurate representation of conditions of thermodynamic equilibrium. Thermodynamic VLE calculations cannot closely reproduce these values, even with  
 170 a higher system pressure (causing a shift of the diagram to higher temperatures) and unreasonably high values for both  $\Delta G^E$  and  $p_{\text{Ag}}^\circ$ .

. The reported uncertainty interval is only based on propagation of the uncertainty in the thermodynamic data of the liquid and gas phases through the model. The resulting uncertainty does not include the effect of operational parameters such as the system temperature and pressure. These are conditions  
 175 that can, in principle, be controlled and the sensitivity of the results to these

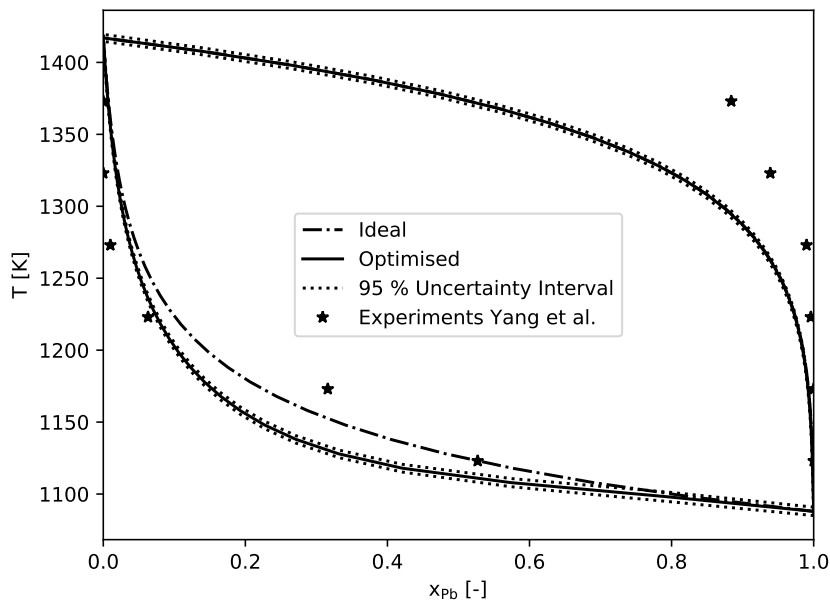


Figure 3: Vapour-liquid diagram for the optimised and ideal Ag-Pb binary alloy at a system pressure of 10 Pa. The 95 % uncertainty interval for the optimised system is shown. Experimental data is obtained from [8].

system parameters can be obtained from a systematic investigation. Their effects can also be obtained from a plot with the system parameter on one axis e.g. the impact of temperature can be quickly obtained from Figs. 3 and 4.

#### 180 4.4. Temperature-independent $\Delta S^E$ for VLE Calculations

. The data compilation of [12] is limited to thermodynamic quantities at a single temperature. Because of this restriction, the preceding calculations necessarily include an assumption of constant enthalpy and excess entropy of mixing. Fortunately, this assumption has a limited impact on the current vapour-liquid  
 185 equilibrium calculations due the the inherent nature of the calculations.

. The impact of the excess entropy and of the related temperature extrapolation for the calculation of the relative volatility (Eq. 4) is diminished due to use of

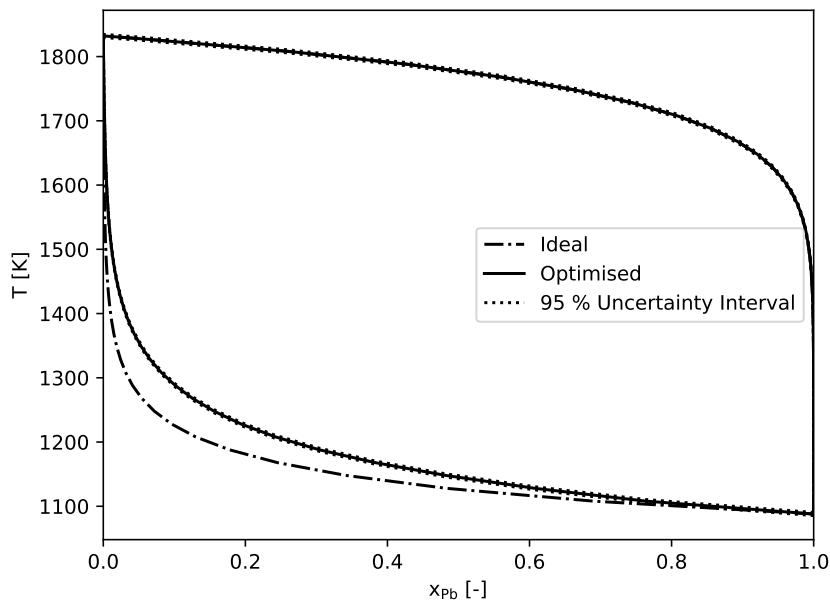


Figure 4: Vapour-liquid diagram for the optimised and ideal Au-Pb binary alloy at a system pressure of 10 Pa. The 95 % uncertainty interval for the optimised system is shown.

the ratio of the activity coefficients. A change with temperature of this ratio will be smaller than the associated change in an individual activity coefficient.

190 The observed decrease in  $\log \alpha$  (Fig 2) is mainly caused by more similar of the saturated vapour pressures at higher temperature.

. For the VLE diagram, the main consideration is to have thermodynamic values with known uncertainties at a temperature in the range directly above the boiling point of the most volatile component: in the case of the Ag-Pb (Fig. 3) and Au-Pb (Fig. 4) VLE diagrams at 10 Pa, this corresponds to a range of 1100–1300 K. The importance of this interval is due to the fact that the effect of non-ideal mixing is most noticeable in this temperature range. The VLE diagram has characteristics that significantly reduce the impact of the extrapolation to other temperatures: 1) there is a negligible impact of  $\Delta G^E$  of the

200 liquid on the vapour curve of an ideal gas, and 2) the boiling points of the pure  
components are not affected by the chemical properties of the liquid phase and  
therefore, any bubble line will terminate in the same two points, regardless of  
the value of  $\Delta G^E$ . This imposes a decrease in impact of the liquid phase mix-  
ing properties on the position of the bubble line, especially as the temperature  
205 increases towards the boiling point of the less volatile component.

## 5. Conclusion

. A methodology is presented by which the reliability of common vapour–liquid  
equilibrium calculations can be assessed. The method takes into account the  
uncertainty in the thermodynamic data for the vapour and liquid phase, and  
210 propagates the uncertainty through the model, so an estimated value and its  
uncertainty interval can be obtained.

. Thermodynamic calculation of Pb removal from Ag–Pb and Au–Pb binary  
liquids is used to illustrate that the chemical interaction between the components  
in the liquid phase has a distinct effect on the vapour–liquid equilibrium. The  
215 excess Gibbs free energy of mixing, when known, should be taken into account  
as it has a significant effect on the position of the bubble line. Any uncertainty  
in this thermodynamic data should not be a barrier for its use, since it can be  
explicitly taken into account for the final result with the methodology presented  
here.

## 220 Acknowledgements

. This research did not receive any specific grant from funding agencies in the  
public, commercial, or not-for-profit sectors.

## Declarations of interest

. None

225 **References**

- [1] J. Deng, Y. Zhang, W. Jiang, Q. Mei, D. Liu, Harmless, industrial vacuum-distillation treatment of noble lead, *Vacuum* 149 (2018) 306–312.
- [2] W. Jiang, C. Zhang, N. Xu, B. Yang, B. Xu, D. Liu, H. Yang, Experimental investigation and modelling of phase equilibria for the Ag–Cu–Pb system in vacuum distillation, *Fluid Phase Equilibria* 417 (2016) 19–24.
- 230 [3] X. Kong, B. Yang, H. Xiong, D. Liu, B. Xu, Removal of impurities from crude lead with high impurities by vacuum distillation and its analysis, *Vacuum* 105 (2014) 17–20.
- [4] T. R. A. Davey, Desilverizing of Lead Bullion, *Journal of Metals* 6 (7) (1954) 838–848.
- 235 [5] T. R. A. Davey, B. Bied-Charreton, Davey Desilverizing Process at Penarroya’s Noyelles–Godault Lead Refinery, *Journal of Metals* 35 (8) (1983) 37–41.
- [6] E. Hála, J. Pick, V. Fried, O. Vilím, *Vapour–Liquid Equilibrium*, 2<sup>nd</sup> English Edition, Pergamon Press, 1967.
- 240 [7] H. Yang, B. Yang, B. Xu, D. Liu, D. Tao, Application of molecular interaction volume model in vacuum distillation of Pb-based alloys, *Vacuum* 86 (2012) 1296–1299.
- [8] H. Yang, C. Zhang, B. Yang, B. Xu, D. Liu, Vapor–liquid phase diagrams of Pb–Sn and Pb–Ag alloys in vacuum distillation, *Vacuum* 119 (2015) 179–184.
- 245 [9] D. V. Malakhov, Confidence intervals of calculated phase boundaries, *Calphad* 21 (3) (1997) 391–400.
- [10] H. L. Lukas, S. G. Fries, Demonstration of the Use of ”BINGSS” With the Mg–Zn System as Example, *Journal of Phase Equilibria* 13 (5) (1992) 532–541.
- 250

- [11] C. B. Alcock, V. P. Itkin, M. K. Horrigan, Vapour Pressure Equations for the Metallic Elements: 298–2500 K, *Canadian Metallurgical Quarterly* 23 (3) (1984) 309–313.
- 255 [12] R. Hultgren, P. D. Desai, D. T. Hawkins, M. Gleiser, K. K. Kelley, Selected Values of the Thermodynamic Properties of Binary Alloys, American Society for Metals, Metals Park, Ohio, 1973.
- [13] I. Karakaya, W. T. Thompson, Alloy Phase Diagrams: Ag–Pb, *Bulletin of Alloy Phase Diagrams* 8 (4) (1987) 397.
- 260 [14] H. Okamoto, Au–Pb (Gold–Lead), *Journal of Phase Equilibria* 14 (5) (1993) 648–649.
- [15] Taylor, Barry N. and Kuyatt, Chriss E., Guidelines for Evaluating and Expressing the Uncertainty of NIST Measurement Results, Tech. Rep. 1297, National Institute of Standards and Technology (1994).
- 265 [16] H. W. Coleman, W. G. Steele, Experimentation, Validation, and Uncertainty Analysis for Engineers, 3rd Edition, John Wiley & Sons, New Jersey, 2009.
- [17] M. H. Kutner, C. J. Nachtsheim, J. Neter, W. Li, Applied Linear Statistical Models, 5th Edition, McGraw-Hill, 2005.
- 270 [18] T. Iida, R. I. L. Guthrie, The Thermophysical Properties of Metallic Liquids. Volume 2: Predictive Models, Oxford University Press, 2015.
- [19] D. R. Lide, CRC Handbook of Chemistry and Physics, 90th Edition, CRC Press, 2010.
- [20] R. O. Williams, Parameterization of the Solution Data for Binary Alloys  
275 by Hultgren et al., *CALPHAD* 15 (1) (1991) 1–10.
- [21] W. McKinney, Python for Data Analysis, O’Reilly, 2013.

## Captions

### 5.1. Figures

1. Plot of the relative volatility  $\alpha$  as function of composition for the Ag–Pb  
280 and Au–Pb binary system, including the 95 % uncertainty interval, at the  
temperatures for which the data was compiled.
2. Effect of temperature on the relative volatility  $\alpha$  at  $x=0.5$  for both binary  
system, including the 95 % uncertainty interval. Values at six tempera-  
285 tures, calculated with the Molecular Interaction Volume Model (MIVM)[7],  
are shown for Au–Pb.
3. Vapour–liquid diagram for the optimised and ideal Ag–Pb binary alloy  
at a system pressure of 10 Pa. The 95 % uncertainty interval for the  
optimised system is shown. Experimental data is obtained from [8].
4. Vapour–liquid diagram for the optimised and ideal Au–Pb binary alloy  
290 at a system pressure of 10 Pa. The 95 % uncertainty interval for the  
optimised system is shown.

### 5.2. Tables

1. Vapour pressure parameters from [11]:  $\log p^\circ(\text{atm}) = A + B T^{-1}$ ; 1 atm  
= 101325 Pa; m.p. = melting point.
- 295 2. Parameters for Eq. 12.
3. Lower triangle of the covariance matrix associated with the application of  
E. 6 to Eq. 12.

Tables

	<i>A</i>	<i>B</i>	T-range (K)
Ag	5.752	-13 827	m.p.-1600
Au	5.832	-18 024	m.p.-2050
Pb	4.911	-9 701	m.p.-1200

	<i>A</i>	<i>B</i>	<i>C</i>
	Ag-Pb		1273 K
$\Delta G^E$ (J)	4441	-2740	4312
$\Delta S^E$ (J/K)	4.810	1.798	9.728
	Au-Pb		1200 K
$\Delta G^E$ (J)	-13279	-1416	7706
$\Delta S^E$ (J/K)	10.805	-1.806	-15.186

	Ag-Pb			Au-Pb		
$\mathcal{C}_{GE}$	4.53e+05	-	-	9.58e+05	-	-
	-2.80e+05	1.73e+05	-	1.02e+05	1.09e+04	-
	4.40e+05	-2.72e+05	4.27e+05	-5.56e+05	-5.93e+04	3.23e+05
$\mathcal{C}_{SE}$	0.38	-	-	2.40	-	-
	0.14	0.05	-	-0.40	0.07	-
	0.77	0.29	1.55	-3.37	0.56	4.73